Accepted Manuscript

The impact of replacement of nitrogen with phosphorus atom in the pyromellitic diimides on their photophysical and electrochemical properties

Sandra Pluczyk, Heather Higginbotham, Przemyslaw Data, Youhei Takeda, Satoshi Minakata

PII: S0013-4686(18)32396-X

DOI: https://doi.org/10.1016/j.electacta.2018.10.156

Reference: EA 32955

To appear in: *Electrochimica Acta*

Received Date: 26 July 2018

Revised Date: 3 October 2018

Accepted Date: 25 October 2018

Please cite this article as: S. Pluczyk, H. Higginbotham, P. Data, Y. Takeda, S. Minakata, The impact of replacement of nitrogen with phosphorus atom in the pyromellitic diimides on their photophysical and electrochemical properties, *Electrochimica Acta* (2018), doi: https://doi.org/10.1016/j.electacta.2018.10.156.

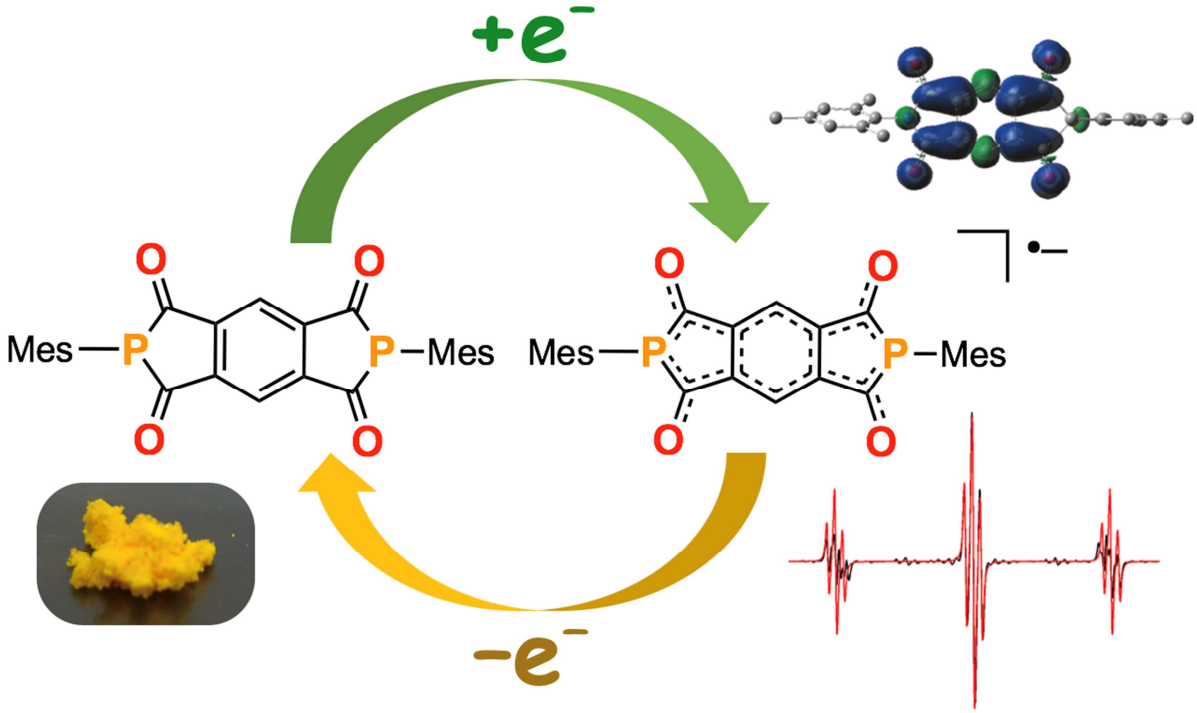

Title. The Impact of Replacement of Nitrogen with Phosphorus Atom in the Pyromellitic Diimides on their Photophysical and Electrochemical Properties

Author names and affiliations. Sandra Pluczyk,[a,*] Heather Higginbotham,[b,*] Przemyslaw Data,[a,b,1] Youhei Takeda,[c,*] Satoshi Minakata[c]

[a] Faculty of Chemistry, Silesian University of Technology, M. Strzody 9, 44-100 Gliwice, Poland

[b] Physics Department, Durham University, South Road, Durham DH1 3LE, United Kingdom

[c] Department of Applied Chemistry, Graduate School of Engineering, Osaka University, Yamadaoka 2-1, Suita, Osaka 565-0871, Japan

[1] ISE member

Corresponding author. Youhei Takeda (e-mail: takeda@chem.eng.osaka-u.ac.jp)

Keywords. phosphorus heterocycles• photophysics • π-conjugated compounds • radical • electrochemistry

Abstract: Exploration of optoelectronic properties of novel phosphorus-embedded π-conjugated compounds would provide us with fundamental information about the design of hitherto unknown electroactive organic materials. Herein, detailed photophysical and electrochemical profiles of a series of benzene-cored diketophosphanyl compounds were investigated with steady- and time-resolved spectroscopic and spectroelectrochemical techniques. The comparative studies revealed the impact of phosphorus and nitrogen atoms on their triplet energies and on the behaviour of electrochemical processes to form radical species.

1. Introduction

The creation of novel main-group element-embedded π-conjugated organic compounds and their building blocks them is vitally important for the development of the next-generation electroactive materials for organic light-emitting diodes (OLEDs), organic photovoltaics (OPVs) and organic field effect transistors (OFETs) [1–4]. Particularly, much attention has been paid to phosphorus-containing π-conjugated compounds, because their optoelectronic properties (e.g., HOMO/LUMO energies, photo-absorption/emission properties, etc.) can be effectively tailored through (C–P)σ*-π* electronic interaction and chemical P-functionalization [5–9]. Making use of their unique physicochemical properties, phosphorus-containing π-conjugated compounds have been utilized as high triplet-energy host materials for OLEDs [10,11] and as emitters [12] in the field of optoelectronics.

As our research program for figuration of phosphorus-containing π-conjugated functional molecules, we focused on aromatic-fused diketophosphanyl compounds [13–18], which are regarded as phosphorus-analogues of rylene and related diimides [19,20]. Although a number of leading literature about the synthesis, structure, and reactivity of diketophosphanyl compounds exist, their physicochemical properties such as photophysical profiles and electrochemical behaviours have been scarcely explored [21–26]. In 2014, the Takeda and Minakata group developed diketophosphanyl compounds **1**, **2**, and **1-O** (Chart 1), and they revealed the fundamental physicochemical properties of the compounds [24]. Importantly, these compounds exhibited distinct positive shifts in reduction potentials (^{red1}E and ^{red2}E) in cyclic voltammograms [24], when compared with their nitrogen analogues, that is, pyromellitic diimides (PyDIs) [27]. More detailed investigations of the impact of pnictogen atoms (P, N) and phosphorus valencies on the physicochemical properties of the diketophosphanyl compounds would provide us with fundamental information about the phosphorus compounds. Herein, we disclose the detailed physicochemical properties of organophosphorus π-conjugated compounds **1**, **2**, and **1-O** (Chart 1), which were revealed with time-resolved spectroscopic, spectroelectrochemical, and EPR techniques.

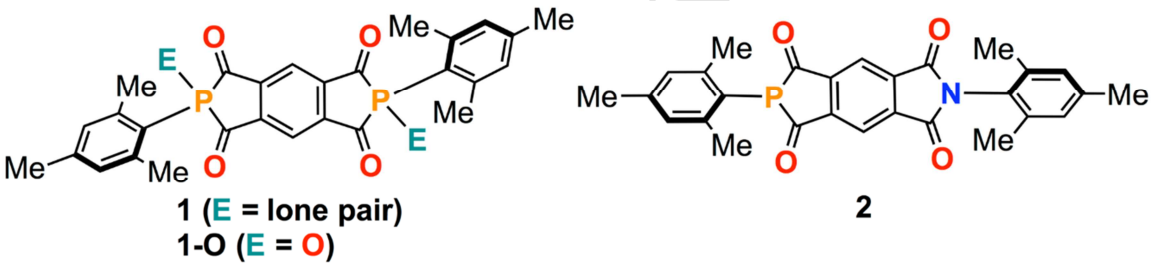

Chart 1. Diketophosphanyl compounds studied in this work.

2. Experimental Methods

2.1 Materials

Diketophosphanyl compounds (**1**, **2**, and **1-O**) were used as the same samples as those used in our previous report [24], which were characterized by ^{1}H, ^{13}C, ^{31}P NMR, IR, LR- and HR-MS spectroscopic techniques.

2.2. Measurements

Steady-state photophysical absorption spectra were recorded with a UV-3600 Shimadzu spectrophotometer, and emission spectra were recorded with a Jobin Yvon Horiba Fluoromax 3. Emission spectra were calibrated for detector efficiency using company supplied, instrument-specific calibration files. Photoluminescence quantum yields were determined with chloroform solutions, using 9,10-diphenyl anthracene as the standard reference dye (Φ = 0.90 in cyclohexane) [28]. The

general method for time-resolved photophysical measurements has been previously described elsewhere [29]. Briefly, the 3rd harmonic of a Nd:YAG laser (355 nm) (EKSPLA-SL312) was used for the measurement of all time-resolved decays with time-resolved spectra collected on a gated intensified charge coupled device CCD camera (Stanford Computer Optics). Samples suitable for analysis were prepared by dropcasting a toluene solution of the phosphorus compounds with zeonex® (1% *w*/*w* ratio) onto clean quartz substrates on a hotplate at 90 °C, and the resulting solid films were dried. All solutions of studied compounds for electrochemical and spectroelectrochemical measurements were prepared in 0.1 M tetrabutylammonium hexafluorophosphate supporting electrolyte (Bu_4NPF_6, TCI > 98%)/dichloromethane (DCM) (Sigma Aldrich ≥99.9%). Electrochemical characterization, as well as EPR spectroelectrochemical studies, were performed in 1 mM, and UV-Vis spectroelectrochemical investigations were carried out with a 0.5 mM solution of investigated materials. For electrochemical characterization, cyclic voltammetry (CV), as well as differential pulse voltammetry (DPV) techniques, were applied. Electrochemical measurements were performed on an Ecochemie AUTOLAB potentiostat-galvanostat model M101, using a typical three-electrode cell. A platinum disk electrode (diameter: 1 mm) was used as a working electrode, a platinum spiral was employed as an auxiliary electrode, and a silver wire was used as a pseudo-reference electrode, with potential being calibrated versus the ferrocene/ferrocenium redox couple. Spectral measurements were carried out using UV-Vis Hewlett Packard spectrophotometer 8453 and JEOL JES-FA 200, X-band CW-EPR spectrometer operating at 100 kHz field modulation. Spectroelectrochemical investigations were conducted with connected spectrometers described above equipped with OMNI or AUTOLAB PGSTAT302N+BA potentiostat. UV-Vis measurements were carried out in a thin layer spectroelectrochemical cell which has a modified cells described in the previous literature [30,31]. An ITO electrode was used as a working electrode, platinum spiral as an auxiliary electrode, and silver wire as a pseudo-reference electrode. EPR measurements were carried out in a cylindrical cell equipped with a platinum wire as a working, platinum spiral as an auxiliary and silver wire as a pseudo-reference electrode. The spectra of the radical anions were recorded during potentiostatic reduction of investigated compounds. The standard based on Mn^{2+} was used for *g*-factor calibration. In order to calculate *g*-factor, the spectra of Mn^{2+} (the third and fourth line) together with investigated samples were measured. The *g*-factor of the investigated sample was calculated based on known values of *g*-factors corresponding to 3rd and 4th lines of Mn^{2+}spectrum (2.03277 for 3rd and 1.98104 for 4th spectral line). The EPR spectra of electrochemically generated radical anions were simulated using WinSim software [32]. All of the investigations were conducted on the solutions purged with argon.

2.3. Theoretical Calculations

All the molecules were geometrically optimized by the DFT method at the UB3LYP/6-311+G(d,p) level of theory using Gaussian 09 package in gas phase [33]. The single point energy calculations were conducted with the optimized geometries at the same theory level. Cartesian coordinates of the initial and the optimized structures are available as xyz files as the Supplementary data.

3. Results and discussion

3.1 Steady-State UV-Vis Spectroscopy

The dilute solutions (methylcyclohexane, toluene, chloroform, and acetonitrile) of phosphorus compounds **1**, **2**, and **1-O** exhibited similar absorption characteristics (Figure S1) to those already reported in the literature (dichloromethane solutions) [24], and to those of other naphthalene-fused diimide compounds, due to their structural similarities. Much like other functionalized naphthalene diimides [34], UV-Vis spectra of **1**, **2**, and **1-O** contain vibronic absorption bands in the range of 200–450 nm (Figure S1). In all absorption spectra, a very strong absorption peak was found in the ultra-violet regime (250–300 nm), indicative of π–π* transitions of the benzene moieties. Additionally, much weaker and lower-energy bands with complex character were observed (λ>400 nm) in all cases, which are associated with charge transfer from the P-Mes groups to the central benzene moieties (Figure S1) [24]. The absorption spectra of **2** were very similar to those previously published [24], highlighting the impact of the nitrogen on the compound's overall character and electronic makeup (Figure S1). The replacement of nitrogen atom with phosphorus atom results in red shift of both absorption bands that are associated with π-π* transition and charge transfer. This shows that the incorporation of phosphorus atom enhances the charge transfer from P–Mes moieties to the benzene core and leads to the narrowing of the band gap of phosphorus compounds, when compared with nitrogen compounds (diimides).

3.2. Time-Resolved Luminescence Spectroscopy

To explore the potential use of these compounds as electroactive materials, detailed photophysical characteristics were investigated with time-resolved spectroscopy (Figure 1 and Figure S2). Almost no emission was observed with the naked eye upon excitation with UV lamp [24]. However, the detailed spectroscopic analysis revealed that all the investigated phosphorus compounds exhibited very weak emission, showing very low quantum yields in solution (less than 1%, in chloroform). Time-resolved/temperature-dependent spectroscopy of the diketophosphanyl molecules put in zeonex® matrix, which were prepared through casting the compounds dispersed in zeonex® matrix at a concentration of 1% *w*/*w*, showed two distinct time regimes; one in nanosecond timescale and the other in micro to millisecond time scale (Figure 1a, c, and e). In all three cases, the emission in

nanosecond region showed similar spectra to those observed with steady-state spectroscopy (Figure 1b, d and f). Therefore, the emission in nanosecond time scale was identified as fluorescence irradiated from the singlet excited state (S_1) to the ground state (S_0). The spectra and the lifetimes (τ) in this nanosecond region are almost constant at all the studied temperatures (Table S1), revealing that these prompt components are unaffected by intramolecular deactivation modes. Comparing the emission spectra of the three molecules at short timescales (2.2 ns after the laser pulse) (black spectra in Figure 1b, d, and f), one can find there is a shift of spectra and the same significant energy variation among **1** (onset wavelength 431 nm; onset energy 2.88 eV), **2** (onset wavelength 395 nm; onset energy 3.17 eV), and **1-O** (onset wavelength 337 nm; onset energy 3.32 eV).

The decay of the prompt emission for all the compounds are mono-exponential with similar τ values between 2.8 ns and 3.3 ns at 280 K (the left components in Figure 1a, c, and e). This highlights the similarity of the conformations of the molecules, which led to indistinct short-lived excited state mechanics. As for the decay profiles of the phosphorus compounds dispersed in the zeonex® matrix, there is a second distinct time-regime in the micro-millisecond region (the right components in Figure 1a, c, and e). At 80 K, each material displays an emission lifetime of >1 ms, which shortens with increasing temperatures. Additionally, the emission spectra at long timescales were bathochromically shifted from the prompt emissions in all the cases (Figure 1b, d, and f). Given their long emission lifetimes, the observed delayed emissions are ascribed to phosphorescence. The phosphorescnece can be identified as the emission from a local triplet state (^{3}LE), due to its non-gaussian profile and vibronic structures, (e.g., phosphorescence spectrum of **2** in Figure 1d). The identity of this long-delay time spectra as phosphorescence was further confirmed by the fact that the emission output and lifetime are highly affected by temperature. The triplet state spectra of **1** (onset wavelength 461 nm; energy onset 2.69 eV) can be seen even at 280 K, subsequently displaying room temperature phosphorescence (RTP) [35]. The similarity of short-lived excited state decay and observation of RTP would suggest conformational rigidity of the compounds and the decrease of the vibrational mode in the molecule. This may attest to the structural rigidity of the compound in the film and fast rates in intersystem crossing to the ^{3}LE, supported by the low quantum yields of fluorescence of solutions at room temperature. N,P-hybrid compound **2** was found to be the most strongly phosphorescent: RTP was observed in zeonex® film [even observed in the steady-state spectrum (Figure S3)] with an onset wavelength of 438 nm (2.83 eV). It should be noted that replacing one phosphorus atom with a nitrogen increases the triplet level of the material. This modularity of the triplet state with slight structural modification might allow for the development of triplet host materials for optoelectronic devices based on the diketophosphanyl scaffolds [36].

In the case of **1-O** dispersed in zeonex® film, two distinct triplet spectra were observed [onset wavelength 461 (2.69 eV) and 419 nm (2.96 eV) (Figure 1f)], both of which were observed at low

temperatures (<200 K). The first triplet state spectrum was found between 63 µs and 7 ms at a low temperature (80 K, red spectrum in Figure 1f), correlating to the low energy triplet state with identical onset energy and spectral shape to the phosphorescence spectrum observed in **1**. Between 7 ms and 89 ms, there was a grow-in of a second weaker triplet state with onset wavelength of 419 nm (2.96 eV; blue spectrum in Figure 1f). These two triplet states within a single material are most likely attributed to the coexistence of two isomeric forms associated with *syn*- and *anti*-conformers with a low and high triplet energy, due to the geometric alteration of the molecule (*vide infra*).

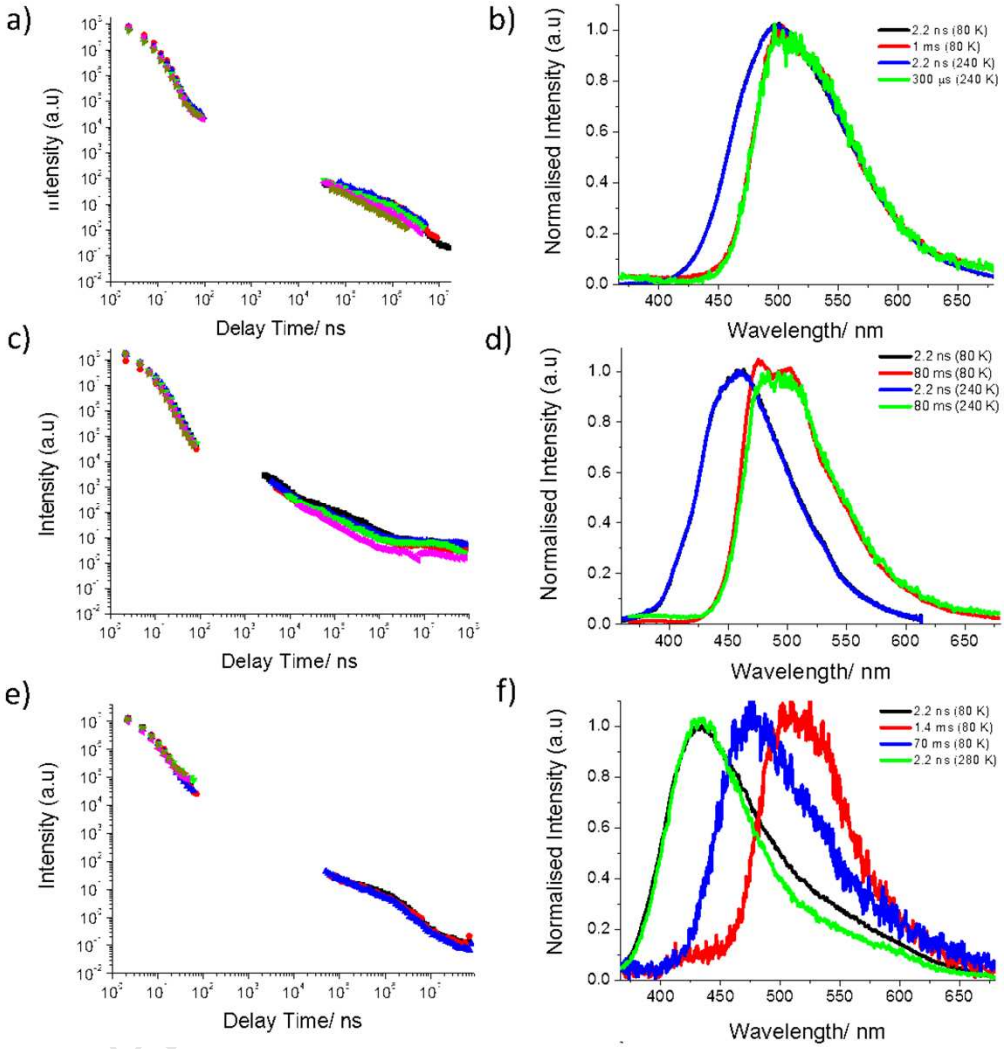

Figure 1. Intensity at varying delay time of 1% *w*/*w* a) **1**, c) **2** and e) **1-O** in zeonex® at 80 K (black), 120 K (red), 160 K (blue), 200 K (green), 240 K (pink), and 280 K (mustard). Corresponding spectra collected at varying delay times and temperatures for b) **1**, d) **2** and f) **1-O.**

3.3 Electrochemistry

In our previous work [24], the basic electrochemical characterization of diketophosphanyl compounds **1**, **2**, and **1-O** was conducted, and obtained results indicated a two-step reduction process

in all investigated compounds. To understand their electrochemical responses, further investigation was conducted. Cyclic voltammogram of **1** showed a similar profile with that previously reported (Figure 2a) [24], while additional peaks were observed in the case of **2** (Figure 2b) and **1-O** (Figure 2c). Compound **2** underwent the first reduction at a slightly lower potential than that for **1** (–1.26 V), and the next reduction occurred at –1.63 V and the third step peaked at –1.85 V (Figure 2b). Notably, the peak observed at –1.63 V (the second reduction) was found extremely sensitive to the presence of oxygen in solution (Figure 3). Therefore, it was impossible to detect this additional process in an insufficiently deoxygenated solution [24]. Figure 3 presents CV voltammograms of compound **2** in solutions with a different degree of deoxygenation, which clearly shows that when the solution is deoxygenated for not enough long time, the 2-step-reduction is observed (Figure 3a and b) like in the previous report in literature [24]. The longer deoxygenation allows us to observe additional, oxygen sensitive, processes. In the previous paper [24] probably they merge into two non-separated peaks. Due to the low solubility of **1-O** in common organic solvents, the registered voltammogram for this compound showed poor signals, not clearly separated (Figure 2c). However, also, in this case, more than two peaks could be distinguished. This was clearly visible on the differential pulse voltammogram (Figure 2d). This measurement allowed to observe four separate peaks at –0.70, –0.85, –1.29, and –1.48 V. Given that trivalent phosphorus compound **1** showed only a two-step reduction in the CV, the multiple step reduction observed for **1-O** would suggest that different conformers are reduced at different potentials due to the geometric alteration of the molecule. It was already shown by time-resolved luminescence spectroscopy that this compound exhibits two triplet states, which is associated with the occurrence of different conformers. In order to confirm it, the geometric modelling was conducted, and which showed the possibility of coexisting of three conformers (Figure S4). Moreover, the simulation of DPV curve was conducted (Figure 4). The DPV curve is fitted with 6 components which are connected with two-step reduction of 3 conformers. This fitting explains also the fact that the peak at –0.85 V is more intense than the other ones, as it is amplified by the signal next to it.

Among investigated molecules, **1-O** underwent the reduction at the highest value of potential, indicating that this compound is the easiest to reduce and it has the highest electron affinity (4.46 eV) (Table 1), whereas compound **2** underwent the reduction at the lowest potential among investigated diketophosphanyl compounds.

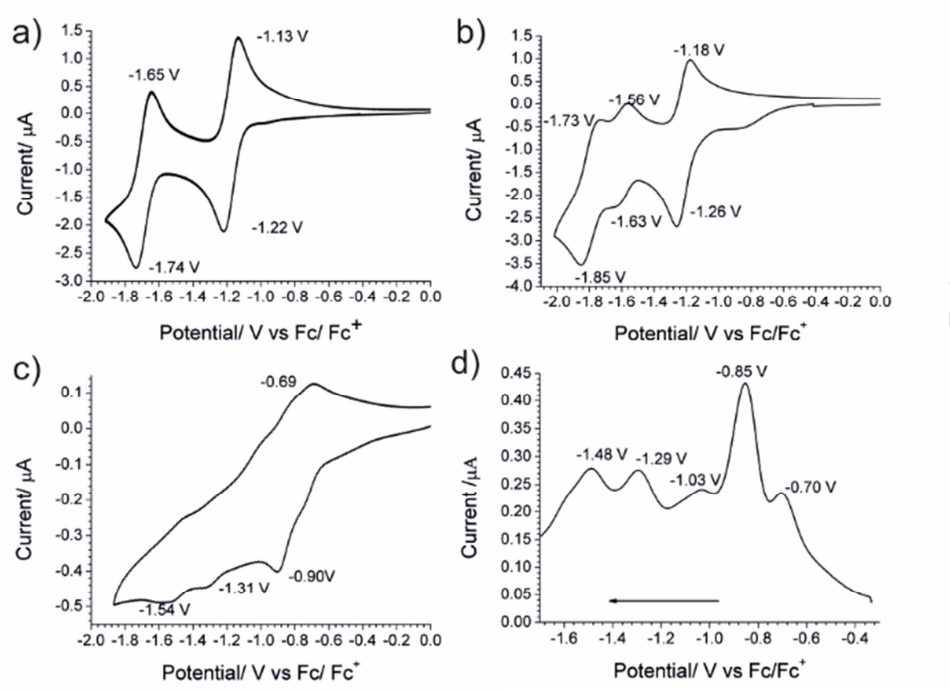

Figure 2. Cyclic voltammogram of a) **1**, b) **2**, c) **1-O**, and d) the differential pulse voltammogram of **1-O** registered in a 0.1 M DCM solution containing Bu_4NPF_6 as the electrolyte. CV registered with a scan rate of 0.10 V/s and DPV with 0.05 V/s. The arrow indicates the direction of working electrode polarization.

Table 1. Summary of electrochemical data.

Compound	E_{onset}[b] [V]	E_{min} [V][b]	EA [eV][a]
1	–1.10	–1.22, –1.74	4.00
2	–1.11	–1.26, –1.63, –1.85	3.99
1-O	–0.64	–0.90, –1.31, –1.54	4.46

[a] EA ~ –LUMO = E_{onset} + 5.10 [eV][37]; [b] Data from CV measurement.

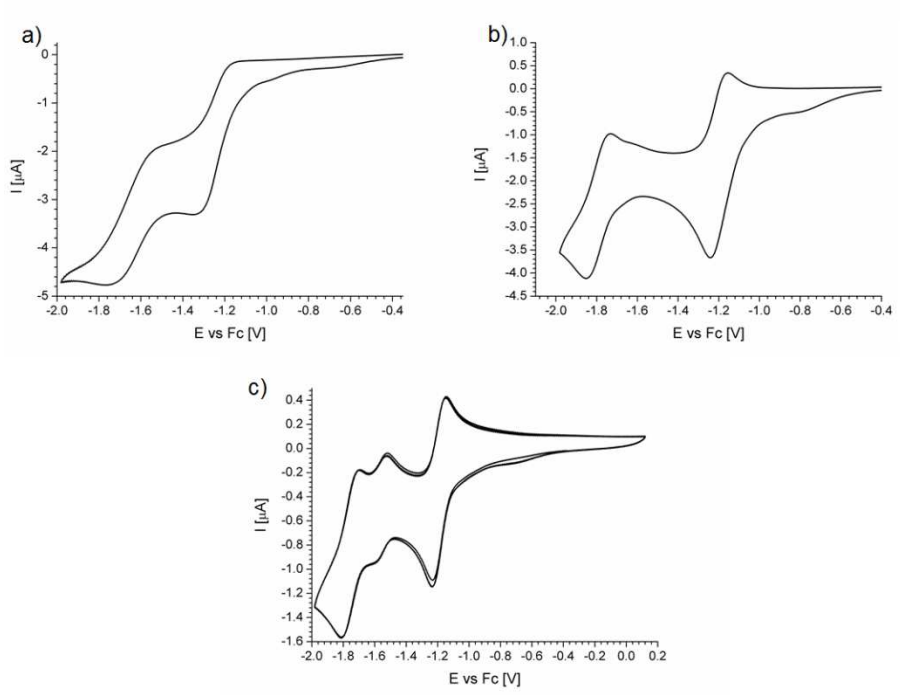

Figure 3. Cyclic voltammograms of compound **2** in solutions with different degrees of deoxygenation. CV registered after purging with argon for a) 3 min, b) 8 min, and c) 23 min.

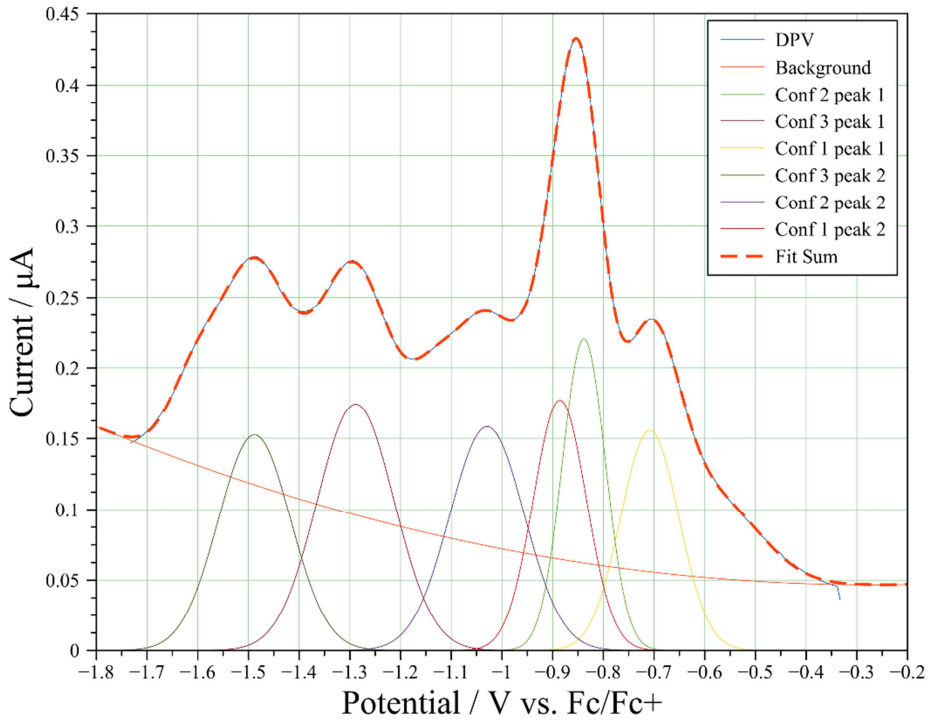

Figure 4. The fitting of DPV curves registered during reduction **1-O** with 6 components corresponding to two-step reductions of 3 conformers.

3.4. UV-Vis-NIR Spectroelectrochemical Investigation

Spectroelectrochemical methods were applied to further analyze the redox processes of the phosphorus compounds. UV-Vis-NIR absorption spectra by varying working electrode potentials in negative sweep mode were collected (Figure 5). Electrochemical reduction of **1** led to the emergence of new two peaks: a broad absorption band covering from 671 up to 834 nm with two maxima at λ_{abs} = 735 and 797 nm, and a narrower peak at around 320 nm (Figure 5a). Likewise, the reduction of **2** gave rise to a broad band from 662 to 792 nm with two maxima (λ_{abs} = 709 and 761 nm) and a peak at 306 nm. Also, the reduction of these compounds led to the shift of bands associated with neutral forms (262 nm for **1**, and 243 nm for **2**): in the case of **1**, the peak gradually decreased in intensity, while the peak of **2** showed only hypsochromic shift, without decreasing in intensity (Figure 5a and 5b). This would be ascribed to the difference in the absorptions of the generated radical anions and neutral forms in these ranges. In the case of compound **2**, probably the radical anion and neutral form exhibit absorptions in the range of 240–243 nm with similar molar absorption coefficients, while in the case of **1** the coefficient for the absorption in the wavelength range for radical anion is much smaller than for neutral form. Based on registered spectra, it could be concluded that replacing a nitrogen atom with a phosphorus atom results in the bathochromic shift of bands associated with not only neutral but also with reduced form. Additionally, the absorption bands observed in the course of reduction can be assigned to generated radical anions, as similar changes in UV-Vis-NIR spectra during reduction of *N*,*N*'-diarylated PyDIs were observed in previous works [38–40]. Due to the low solubility of **1-O** in organic solvents, it was difficult to obtain spectroelectrochemical spectra.

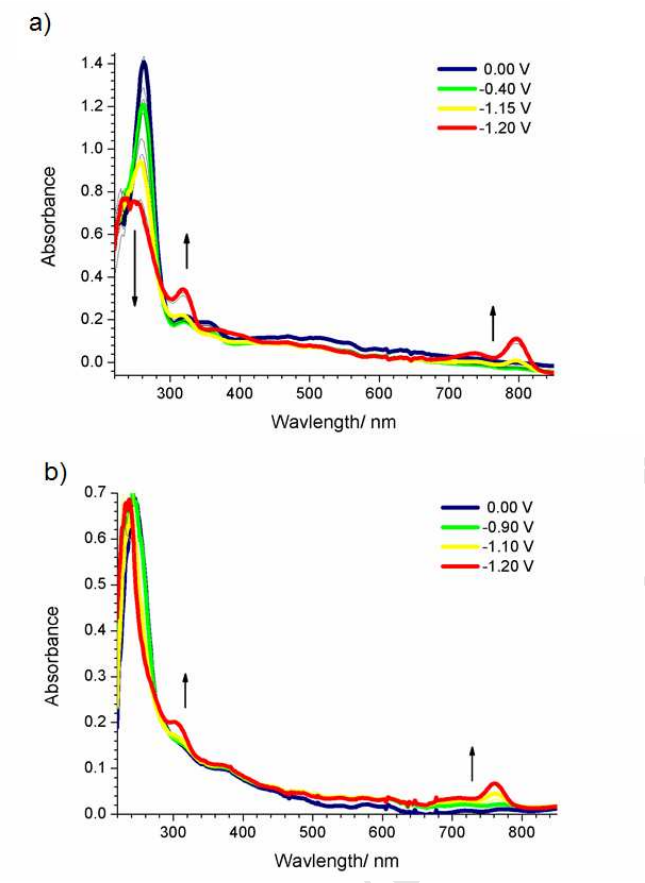

Figure 5. UV-Vis-NIR spectra collected at negative working electrode potentials for the DCM solutions of a) **1** and b) **2** (*c*: 0.1 M, electrolyte: Bu_4NPF_6)

3.5. EPR Spectroelectrochemistry

Electron paramagnetic resonance (EPR) spectroelectrochemistry was employed to further explore the nature of generated species through electrochemical reduction of the phosphorus compounds. The reduction of all investigated molecules allowed for the registration of EPR spectra (Figure 6–8), which confirmed the generation of radical anions. All registered spectra showed hyperfine structures, and from the set of hyperfine coupling constants (hfcc: *a*), the localization of unpaired spin density was implicated. In the case of **1**, the first step of reduction led to the generation of radical anion $\mathbf{1}^{\bullet-}$, whose radical spin localizes on the central benzene core, supported by the EPR spectra (Figure 6a): the main signal is a result of hyperfine coupling with two equivalent ^{31}P nuclei (I = 1/2) and two equivalent ^{1}H nuclei (I = 1/2) (Figure 6a and Table 2), which was supported by the spin density isosurface calculated with the DFT method (Figure 6b). Since P-pyramidal inversion of **1** is very rapid in solution even at room temperature [24], the registered spectra would consist of signals derived from two radicals associated with *syn*- and *anti*-conformers. Therefore, additional small triplets could be attributed to the minor conformer radical (Figure S5 and Table 2). Further decreasing

of the working electrode potential up to the second step of reduction of **1** led to the generation of spin-less dianion species.

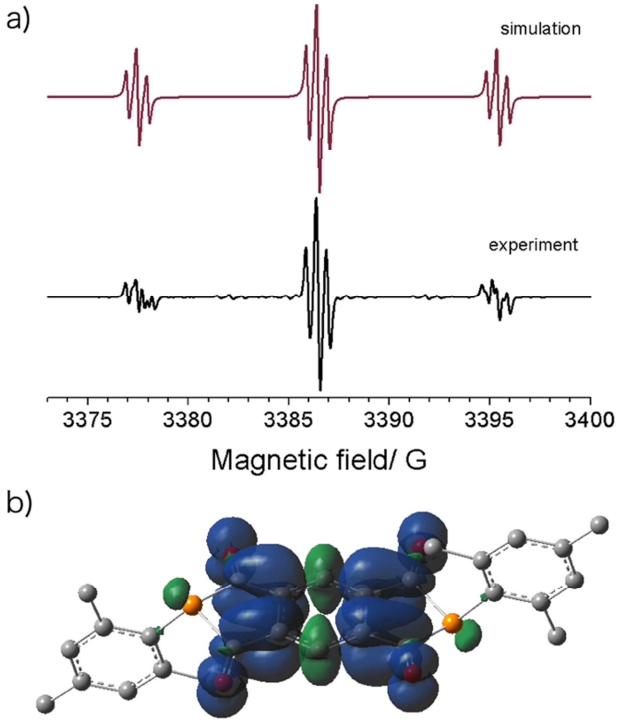

Figure 6. a) EPR spectra registered during the reduction of **1** and the simulated spectra corresponding to one radical interaction; b) the spin density isosurface (isosurface = 0.0004 e/Å^3) of **1**$^{\bullet-}$ (*anti*) calculated at the UB3LYP/6-311+G(d,p) level.

As shown in the CV measurement, the reduction of N,P-hybrid **2** occurs in a three-stage process. The EPR spectrum registered at –1.25 V suggested that the first reduction step generated radical anion **2**$^{\bullet-}$ in which unpaired spin interacts via ^{31}P, one ^{14}N (I = 1), and two ^{1}H nuclei of the central benzene core (Figure 7a and Table 2). Notably, further electrochemical reduction at a lower potential (–1.79 V) led to change in EPR spectra: doublet of multiplets, which was the result of the first-step reduction, decreased in intensity, and a new set of multiplet between these doublets appeared (Figure 7b). The potential at which the EPR spectra of **2**$^{\bullet3-}$ was registered (–1.79 V) was set at the value between the second (–1.63 V) and third (–1.85 V) peaks on the CV (Figure 2b), as the firstly generated radical anion **2**$^{\bullet-}$ had to be reduced to the spin-less (EPR silent) dianion **2**$^{2-}$, and which thereafter further reduced to the second anion radical **2**$^{\bullet3-}$. Based on this measurement, it would be very difficult to clearly state whether or not the second and the third reduction peaks on CV are connected with the generation of **2**$^{2-}$ or **2**$^{\bullet3-}$ species, respectively, because these reduction peaks on the CV locate too close to each other. However, these results can explain the multi-steps reduction processes which involve the generation of two different radical anions **2**$^{\bullet-}$ and **2**$^{\bullet3-}$. Simulation of EPR lineshape of the new signal (Figure 7b and Table 2) indicated that the secondly generated radical would interact with the same set

of atoms for $\mathbf{2}^{\bullet-}$, but different hfcc values were obtained (Table 2). The radical anion generated as a result of the first reduction mostly interacts with ^{31}P nucleus [a (^{31}P) = 10.87 G; a (^{14}N) = 1.01 G], which were also supported with the DFT calculation results [a_{cal} (^{31}P) = 10.68 G; a_{cal} (^{14}N) = 1.06 G] (Table S8). In sharp contrast, the further reduction gave rise to a radical species which does not localize on the ^{31}P nucleus [a (^{31}P) = 0.18], while the coupling constant for ^{14}N nucleus increased to 1.99 G (Table 2). These results would indicate that the reduction to $\mathbf{2}^{\bullet 3-}$ occurred mostly on the imide side.

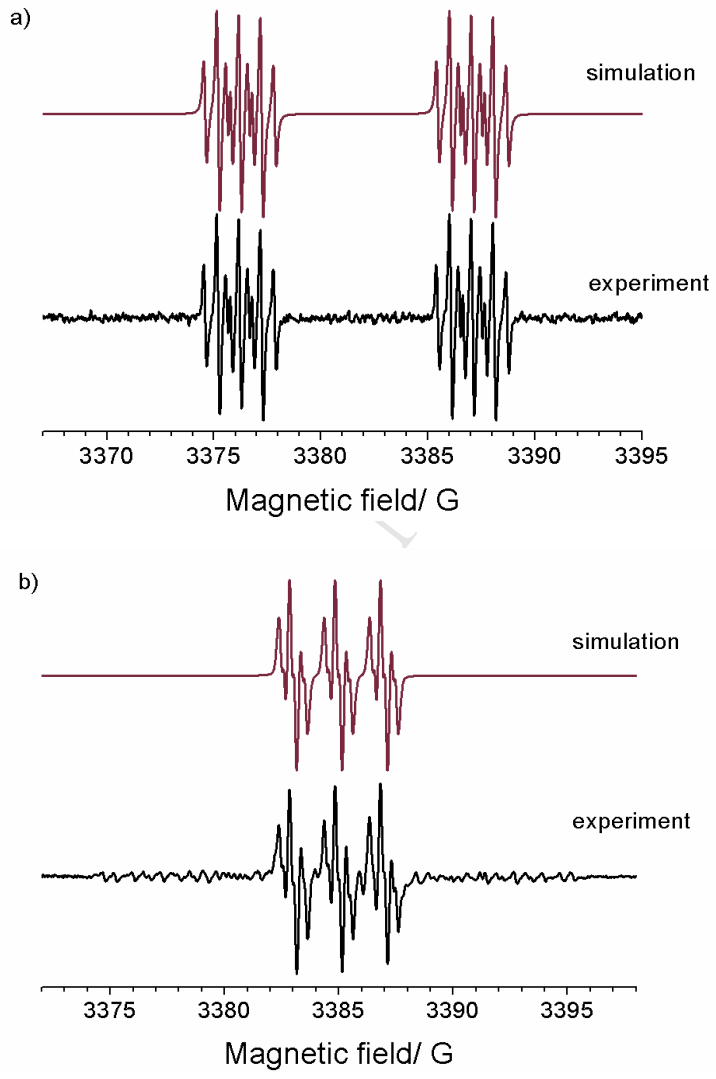

Figure 7. Registered EPR spectra and the simulations of a) $\mathbf{2}^{\bullet-}$ and b) $\mathbf{2}^{\bullet 3-}$.

Table 2. Fitting parameters for the simulation of EPR spectra together with *g*-factors estimated from experimental spectra.

Radical	*a* [G]	Linewidth [G]	*g*-factor

	^{31}P(1): 8.96, 8.96; ^{1}H: 0.51, 0.51	0.12	
1$^{\bullet-}$			2.0046
	^{31}P(2): 6.00, 3.75; ^{1}H: 0.51, 0.51	0.10	
2$^{\bullet-}$	^{14}N: 1.01; ^{31}P: 10.87; ^{1}H: 0.61, 0.61	0.10	2.0045
2$^{\bullet 3-}$	^{14}N: 1.99; ^{31}P: 0.18; ^{1}H: 0.46, 0.46	0.10	2.0041
1-O$^{\bullet-}$	—	—	2.0038
1-O$^{\bullet 3-}$	^{31}P: 0.47, 0.45; ^{1}H: 0.03, 0.17	0.08	2.0038

The reduction of **1-O** also resulted in radical species, which was clearly confirmed by EPR spectroscopy (Figure 8). Due to the low solubility in organic solvents, it was difficult to obtain well-resolved spectra with reasonable intensity (Figure S6), and therefore it did not allow for unambiguous analysis of radical anion interactions. Nevertheless, based on the EPR spectroelectrochemical results, it could be concluded that the reduction of **1-O** leads to the generation of radical anion (**1-O**$^{\bullet-}$) (Figure S6), which underwent further reduction to dianion, and after that to another radical anion (**1-O**$^{\bullet 3-}$) (Figure 8 and Table 2). In the case of **1-O**$^{\bullet-}$, the hyperfine structure was not fitted, due to the fact that the registered spectrum was not resolved enough (Figure S6), while the simulation of the hyperfine structure of EPR spectra of **1-O**$^{\bullet 3-}$ showed the radical interactions with both phosphorus as well as hydrogen nuclei (Figure 8 and Table 2).

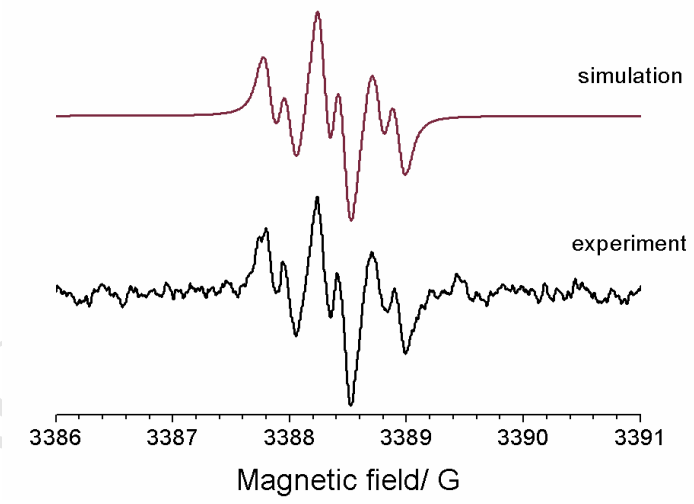

Figure 8. Registered EPR spectra and the simulations of **1-O**$^{\bullet 3-}$.

4. Conclusions

Detailed photophysical and electrochemical properties of a series of phosphorus analogues of PyDIs were investigated. The replacement of nitrogen with phosphorus atom results in red shift of absorptions in the low energy region, leading to the enhancement of the charge transfer character from

the P–Mes groups to the benzene core and to the narrowing of the band gaps, when compared with nitrogen compounds. All the materials showed weak emissions in solution (less than 1% of quantum yield). Time-resolved spectroscopy in the zeonex® matrix (1% *w/w*) shows two distinct time regimes: the one in nanosecond and the other in micro to millisecond timescales. In the nanosecond time scale, the emission is bathochromically shifted. The emission at long timescale was found out to be phosphorescence. Importantly, the photophysical analysis revealed that the substitution of a phosphorus atom with a nitrogen entity allows for tailoring the triplet energy. The compound with a nitrogen and a phosphorus atom **2** exhibited the most strong phosphorescence and showed the higher triplet energy than that of **1**. Amassing this feature with their predictable HOMO/LOMO energies and their extremely low fluorescence emissions, these materials are potentially useful as host materials for electroactive applications. All investigated compounds were found to undergo multi-step electrochemical reductions. Replacement of nitrogen with a phosphorus atom led to the increase in reduction potential, showing the phosphorus-containing organic materials as a promising alternative for well-known bisimide organic electron-acceptor materials, as they may exhibit even lower LUMO levels than those of bisimides. This would allow for designing new stable electron acceptors or ambipolar materials for organic electronics application. The spectroelectrochemical analysis led to the determination of the nature of reduced species of the phosphorus compounds. The first reduction step generated radical anion species. In the case of **1**, reduction proceeds as a two-steps process. The first reduction stage would be connected with radical anion formation, which then in course of the second reduction was transferred to the formation of spin-less dianion. In the case of **2** and **1-O**, the reduction was three- and four-steps process, respectively. In both cases, radical anions generated in the first reduction was further transferred into another radical species. In the case of **2**, the first step of reduction involves mostly on the phosphorus nucleus, whereas the reduction to $\mathbf{2}^{\bullet 3-}$ on the nitrogen nucleus.

Acknowledgements

Information included in this publication was obtained through the networking action funded from the European Union's Horizon 2020 research and innovation programme under grant agreement No. 691684 project ORZEL. This work was partly supported by a Grant-in-Aid for Scientific Research on Innovative Areas "π-System Figuration: Control of Electron and Structural Dynamism for Innovative Functions" from Japan Society for the Promotion of Science (JSPS) (JP15H0099, JP17H05155, to YT) and by the Shorai Foundation for Science and Technology (to YT).

Appendix A. Supplementary data

Supplementary data associated with this article can be found in the online version.

References

[1] A. Fukazawa, S. Yamaguchi, Ladder π-conjugated materials containing main-group elements, Chem.—Asian J. 4 (2009) 1386–1400.

[2] X. He, T. Baumgartner, Conjugated main-group polymers for optoelectronics, RSC Adv. 3 (2013) 11334–11350.

[3] S. M. Parke, M. P. Boone, E. Rivard, Marriage of heavy main group elements with π-conjugated materials for optoelectronic applications, Chem. Commun. 52 (2016) 9485–9505.

[4] A. M. Priegert, B. W. Rawe, S. C. Serin, D. P. Gates, Polymers and the p-block elements, Chem. Soc. Rev. 45 (2016) 922–953.

[5] T. Baumgartner, R. Réau, Organophosphorus π-conjugated materials, Chem. Rev. 106 (2006) 4681–4727.

[6] M. Stolar, T. Baumgartner, Phosphorus-containing materials for organic electronics, Chem.—Asian J. 9 (2014) 1212–1225.

[7] M. A. Shameem, A. Orthaber, Organophosphorus compounds in organic electronics, Chem.—Eur. J. 22 (2016) 10718–10735.

[8] R. Szűcs, F. Riobé, A. Escande, D. Joly, P.-A. Bouit, L. Nyulászi, M. Hissler, Strategies toward phosphorus-containing PAHs and the effect of P-substitution on the electronic properties, Pure Appl. Chem. 89 (2017) 341–355.

[9] R. Szűcs, P.-A. Bouit, L. Nyulászi, M. Hissler, Phosphorus-containing polycyclic aromatic hydrocarbons, ChemPhysChem 18 (2017) 2618–2630.

[10] J. Zhang, D. Ding, Y. Wei, H. Xu, Extremely condensing triplet states of DPEPO-type hosts through constitutional isomerization for high-efficiency deep-blue thermally activated delayed fluorescence diodes, Chem. Sci. 7 (2016) 2870–2882.

[11] S. Y. Lee, C. Adachi, T. Yasuda, High-efficiency blue organic light-emitting diodes based on thermally activated delayed fluorescence from phenoxaphosphine and phenoxathiin derivatives, Adv. Mater. 28 (2016) 4626–4631.

[12] C. Fave, T.-Y. Cho, M. Hissler, C.-W. Chen, T.-Y. Luh, C.-C. Wu, R. Réau, First examples of organophosphorus-containing materials for light-emitting diodes, J. Am. Chem. Soc. 125 (2003) 9254–9255.

[13] V. K. Issleib, K. Mohr, H. Sonnenschein, Cyclische carbonsäurephosphide, Z. Anorg. Allg. Chem. 408 (1974) 266–274.

[14] D. Fenske, E. Langer, M. Heymann, H. J. Becher, Phenylbis(trimethylsilyl)phosphin und 1,2-diphenyl-1,2-bis(tri-methylsilyl)diphosphan als reagenzien zur darstellung von phosphorheterocyclen und acylphosphinen, Chem. Ber. 109 (1976) 359–362.

[15] C. L. Liotta, M. L. McLaughlin, D. G. van Derveer, B. A. O'Brien, The 2-*H*-isophosphindoline-1,3-dione ion: the phosphorus analogue of the phthalimide anion, Tetrahedron Lett. 25 (1984) 1665–1668.

[16] A. R. Barron, S. W. Hall, A. H. Cowley, Cyclic carboxylic monophosphides: a new class of phosphorus, J. Chem. Soc., Chem. Commun. (1987) 1753–1754.

[17] A. Decken, E. D. Gill, F. Bottomley, 2-Phenyl-isophosphindoline-1,3-dione, Acta Crystallogr. Sect. E: Struct. Rep. Online 60 (2004) o1456–o1457.

[18] A. J. Saunders, I. R. Crossley, M. P. Coles, S. M. Roe, Facile self-assembly of the first diphosphametacyclophane, Chem. Commun. 48 (2012) 5766–5768.

[19] S. V. Bhosale, C. H. Jani, S. J. Langford, Chemistry of naphthalene diimides, Chem. Soc. Rev. 37 (2008) 331–342;

[20] X. Zhan, A. Facchetti, S. Barlow, T. J. Marks, M. A. Ratner, M. R. Wasielewski, S. R. Marder, Rylene and related diimides for organic electronics, Adv. Mater. 23 (2011) 268–284.

[21] X. He, J. Borau-Garcia, A. Y. Y. Woo, S. Trudel, T. Baumgartner, Dithieno[3,2-*c*:2′,3′-*e*]-2,7-diketophosphepin: a unique building block for multifunctional π-conjugated materials, J. Am. Chem. Soc. 135 (2103) 1137–1147.

[22] X. He, T. Baumgartner, Synthesis and properties of a dicationic π-extended dithieno[3,2-*c*:2′,3′-*e*]-2,7-diketophosphepin, Organometallics 32 (2013) 7625–7628.

[23] S. Sánchez, A. Y. Y. Woo, T. Baumgartner, Electron-accepting π-conjugated species with 1,8-naphthalic anhydride or diketophosphanyl units, Mater. Chem. Front. 1 (2017) 2324–2334.

[24] Y. Takeda, T. Nishida, S. Minakata, 2,6-Diphospha-*s*-indacene-1,3,5,7(2*H*,6*H*)-tetraone: a phosphorus analogue of aromatic diimides with the minimal core exhibiting high electron-accepting ability, Chem.—Eur. J. 20 (2014) 10266–10270.

[25] Y. Takeda, T. Nishida, K. Hatanaka, S. Minakata, Revisiting phosphorus analogues of phthalimides and naphthalimides: syntheses and comparative studies, Chem.—Eur. J. 21 (2015) 1666–1672.

[26] Y. Takeda, K. Hatanaka, T. Nishida, S. Minakata, Thieno[3,4-c]phosphole-4,6-dione: a versatile building block for phosphorus-containing functional π-conjugated systems, Chem.—Eur. J. 22 (2016) 10360–10364.

[27] Q. Zheng, J. Huang, A. Sarjeant, H. E. Katz, Pyromellitic diimides: minimal cores for high mobility n-channel transistor semiconductors, J. Am. Chem. Soc. 130 (2008) 14410–14411.

[28] S. Hamai, F. Hirayama, Actinometric determination of absolute fluorescence quantum yields, J. Phys. Chem. 87 (1983) 83–89.

[29] C. Rothe, A. P. Monkman, Triplet exciton migration in a conjugated polyfluorene, Phys. Rev. B 68 (2003) 075208.

[30] W. Kaim, J. Fiedler, Spectroelectrochemistry: the best of two worlds. Chem. Soc. Rev. 38 (2009) 3373–3382.

[31] M. Gora, S. Pluczyk, P. Zassowski, W. Krzywiec, M. Zagorska, J. Mieczkowski, A. Pron, EPR and UV–vis spectroelectrochemical studies of diketopyrrolopyrroles disubstituted with alkylated thiophenes, Synth. Met. 216 (2016) 75–82.

[32] D. R. Duling, Simulation of multiple isotropic spin-trap EPR spectra, J. Magn. Reson. Ser. B 104 (1994) 105–110.

[33] Gaussian 09, Revision A.02, M. J. Frisch, G. W. Trucks, H. B. Schlegel, G. E. Scuseria, M. A. Robb, J. R. Cheeseman, G. Scalmani, V. Barone, B. Mennucci, G. A. Petersson, H. Nakatsuji, M. Caricato, X. Li, H. P. Hratchian, A. F. Izmaylov, J. Bloino, G. Zheng, J. L. Sonnenberg, M. Hada, K. Ehara, K. Toyota, R. Fukuda, J. Hasegawa, M. Ishida, T. Nakajima, Y. Honda, O. Kitao, H. Nakai, T. Vreven, J. A. Montgomery Jr., J. E. Peralta, F. Ogliaro, M. Bearpark, J. J. Heyd, E. Brothers, K. N. Kudin, V. N. Staroverov, R. Kobayashi, J. Normand, K. Raghavachari, A. Rendell, J. C. Burant, S. S. Iyengar, J. Tomasi, M. Cossi, N. Rega, J. M. Millam, M. Klene, J. E. Knox, J. B. Cross, V. Bakken, C. Adamo, J. Jaramillo, R. Gomperts, R. E. Stratmann, O. Yazyev, A. J. Austin, R. Cammi, C. Pomelli, J. W. Ochterski, R. L. Martin, K. Morokuma, V. G. Zakrzewski, G. A. Voth, P. Salvador, J. J. Dannenberg, S. Dapprich, A. D. Daniels, O. Farkas, J. B. Foresman, J. V. Ortiz, J. Cioslowski, D. J. Fox, Gaussian, Inc., Wallingford CT, 2009.

[34] F. Würthner, S. Ahmed, C. Thalacker, T. Debaerdemaeker, Core-substituted naphthalene bisimides: new fluorophors with tunable emission wavelength for FRET studies, Chem.—Eur. J. 8 (2002) 4742–4750.

[35] S. Mukherjee, P. Thilagar, Recent advances in purely organic phosphorescent materials, Chem. Commun. 51 (2015) 10988–11003.

[36] Y. Tao, C. Yang, J. Qin, Organic host materials for phosphorescent organic light-emitting diodes, Chem. Soc. Rev. 40 (2011) 2943–2970.

[37] C. M. Cardona, W. Li, A. E. Kaifer, D. Stockdale, G. C. Bazan, Electrochemical considerations for determining absolute frontier orbital energy levels of conjugated polymers for solar cell applications, Adv. Mater. 23 (2011) 2367–2371.

[38] S. F. Rak, T. H. Jozefiak, L. L. Miller, Electrochemistry and near-infrared spectra of anion radicals containing several imide or quinone groups, J. Org. Chem. 55 (1990) 4794–4801.

[39] D. Gosztola, M. P. Niemczyk, W. Svec, A. S. Lukas, M. R. Wasielewski, Excited doublet states of electrochemically generated aromatic imide and diimide radical anions, J. Phys. Chem. A 104 (2000) 6545–6551.

[40] S. Pluczyk, P. Zassowski, R. Rybakiewicz, R. Wielgosz, M. Zagorska, M. Lapkowski, A. Pron,

1 UV-vis and EPR spectroelectrochemical investigations of triarylamine functionalized arylene bisimides,
2 RSC Adv. 5 (2015) 7401–7412.